THE ASTROPHYSICAL JOURNAL, 412:489–503, 1993 August 1

SPARTAN 1 X-RAY OBSERVATIONS OF THE PERSEUS CLUSTER. III. THE DISTRIBUTION OF IRON IN THE INTRACLUSTER GAS

M. P. KOWALSKI, R. G. CRUDDACE, W. A. SNYDER, AND G. G. FRITZ
E. O. Hulburt Center for Space Research, Naval Research Laboratory, Code 7620, Washington, DC 20375-5352
M. P. ULMER
Department of Physics and Astronomy, Northwestern University, Evanston, IL 60208
AND
E. E. FENIMORE
Los Alamos National Laboratory, MS D436, Los Alamos, NM 87545
Received 1992 February 21; accepted 1993 February 4

ABSTRACT

The Spartan 1 instrument has resolved the spatial and spectral distribution of the 1–10 keV X-ray emission from the Perseus cluster in a region extending 50′ (1.6 Mpc) from the center. The data were fitted with a spherically symmetric three-dimensional model which included separate components for the cooling flow, the extended cluster emission, and a possible point source located at NGC 1275. A careful study has been made of the abundance distribution of iron as a function of radius. We confirm the existence of a gradient where the best-fit central abundance is $0.77^{+0.30}_{-0.38}$ times the solar value and the linear gradient is $-1.10^{+0.89}_{-2.24}$ Mpc^{-1} (90% confidence for a single interesting parameter in both cases). Joint 90% confidence limits to the abundance parameters have been established, and the resulting limits to the abundance distribution have been applied to theoretical models of cluster structure and evolution. We find that our results are consistent with a gas-removal mechanism with enhanced efficiency at the cluster center such as ram-pressure stripping or thermal exaporation. Our results are also in agreement with cluster evolution models in which the initial density of primordial gas in the cluster formation region is high ($\geq 10^{28}$ g cm^{-3}). The integrated mass of iron out to a radius of 1.6 Mpc is about 3×10^{10} $M_\odot$, about 5 times smaller than that deduced from X-ray observations under the assumption of a constant abundance.

Subject headings: galaxies. abundances — galaxies: clustering — intergalactic medium — X-rays: galaxies

1. INTRODUCTION

The detection of iron K-line emission in the Perseus cluster of galaxies has established that the dominant source of X-rays is a hot intracluster gas emitting thermal bremsstrahlung radiation (Mitchell et al. 1976; Serlemitsos et al. 1977). Taken as an average over the whole cluster, the gas is found to have an iron abundance of about 0.4 times the solar value, $A_\odot$. However, these observations were made with instruments which had wide fields of view and no spatial resolution. Although the Perseus cluster has been mapped carefully in broad low-energy bands by imaging instruments (Branduardi-Raymont et al. 1981; Fabian et al. 1981), until recently no observations had been made which simultaneously achieved spatial and spectral resolution over a broad region of the cluster in a wide energy band (1–10 keV). Such measurements hold the key to determining the structure and evolution of cluster gas as derived from the density, temperature, and abundance distributions.

Spartan 1 was one of the first instruments designed to provide such observations. In an earlier paper describing Spartan 1 results (Ulmer et al. 1987), we reported on the average spectra of two regions centered on NGC 1275: a region of radius 5′ (0.16 Mpc for $z = 0.0183$, $H_0 = 50$ km s^{-1} Mpc^{-1}) surrounding NGC 1275 and dominated by the cluster cooling flow, and an external shell having inner and outer radii of 6′ and 20′ (0.2–0.6 Mpc). The results contained marginal evidence for a decrease in iron abundance with radius, in that the inner and outer regions yielded abundances of $0.81^{+0.26}_{-0.16}$ and $0.41^{+0.41}_{-0.25}$ $A_\odot$, respectively. More recently we published the results of fitting a three-dimensional model to the radial distributions of broad-band surface brightness and hardness ratio (Snyder et al. 1990). In that work we extended the analysis to the maximum radius reached by the data, 50′, but omitted the cooling flow region and assumed a constant abundance of 0.5 $A_\odot$. Here we reexamine the abundance-radius relation with more detailed models and fit the entire range (0′–50′) of the Spartan 1 data. We compare our results to those of other missions, including the coded-aperture X-ray telescope flown on the shuttle Spacelab 2 mission (Ponman et al. 1990; Eyles et al. 1991) and the BBXRT solid-state X-ray spectrometer flown on the shuttle Astro mission (Petre 1991), and we examine what our results imply about cluster structure and evolution.

2. OBSERVATIONS

Spartan 1 was deployed on orbit by the shuttle Discovery on 1985 June 20 (Cruddace et al. 1989). The free-flying payload contained two coaligned X-ray proportional counters (Fritz et al. 1992), each with a 1–12 keV bandpass, 660 cm^2 effective area, 16% energy resolution at 6 keV, and two coaligned rectangular collimators. Each collimator has a 5′ × 3° FWHM field of view with an approximately triangular response in both directions. During the 2 day mission observations were made of the Galactic center (Kawai et al. 1988; Snyder et al. 1991) and the Perseus cluster, in which the collimator field was scanned at a uniform rate across each source in a direction perpendicular to the long collimator axis. To obtain uniform angular coverage the scan angle was changed each orbit, and in the case of the Perseus cluster, NGC 1275 was placed at the center of the scan pattern (Synder et al. 1990).

Details of the aspect solution, the determination of the background, and analyses of the errors can be found in Fritz et al. (1993) and Snyder et al. (1990). Data were screened to reject periods of high background or poor aspect solution, and about 11 ks of good data on Perseus remain after screening. Pulse-height information both on- and off-source was examined for nonlinear channels, which were eliminated subsequently from the analysis. The data base used in this investigation has an energy range of 1–9.5 keV and spans radii up to 50′ from the cluster center. In this data base background has been subtracted and the counts grouped radially in bins centered on NGC 1275.

The results may be influenced by errors in background subtraction, measurement of the collimator response, the aspect solution, and detector calibration. We have estimated these systematic errors (Snyder et al. 1990; Fritz et al. 1993), and we discuss here the resulting uncertainties in our analysis. The Spartan 1 background is derived from a correlation between coincidence counts and background counts obtained when the instrument was not viewing an X-ray source, and therefore to take into account possible systematic errors in the background we have added in quadrature the uncertainty in this correlation to the statistical error.

The collimator response function is approximately triangular in both the scan direction and perpendicular to it. We have calibrated the response of all collimators (2 per detector) in both directions by tests in the laboratory and in particular by scanning the point source Sco X-2 during flight (Fritz et al. 1993). The peak transmission efficiency of the two collimator banks was 55%. Our results are most sensitive to the response function in the scan direction, which we have determined by fitting a fourth-order polynomial to the Sco X-2 scan. The half-widths at zero amplitude of the two response functions were 5′.81 and 5′.49, respectively, and we have determined using simulations that uncertainties in these values should have no significant influence on our results. The positional uncertainty in the aspect solution is about 30″ at the cluster center and rises to 60″ at 50′. These uncertainties are small compared to the collimator width, and in addition their effect on the results is reduced by radially binning the data.

The energy-to-pulse-height calibration was measured in the laboratory before and after flight using Fe^{55} and other fluorescent sources, while monitoring of gain variations during flight was accomplished using an on-board Fe^{55} source. Differential nonlinearity in the pulse height analyzer was measured in the laboratory, and values of 3% at 1 keV and less than 1% at energies greater than 2 keV were obtained. Uncertainties in the thicknesses of the detector window materials and in the detector gas pressure and temperature are small and introduce negligible errors to our analyses. Likewise, uncertainties in photoelectric absorption coefficients (Viegele 1973) and interstellar absorption coefficients (Brown & Gould 1970) used in the modeling introduce relatively small errors.

In fitting the data to models of the cluster, an error budget was kept for all subroutines within the modeling program, especially those dealing with numerical integrations, and the total error in model count rates is less than 8%. Simulations have shown that the model's best-fit parameter values and confidence intervals are not sensitive to errors of this size.

We have searched for systematic differences between the two Spartan 1 detectors by fitting the data from each detector separately. Most best-fit parameter values obtained from the data of either detector alone are nearly identical to the results obtained from the data summed from both detectors and in all cases lie within the confidence interval obtained from the summed data. As was to be expected, the parameter errors were slightly larger.

3. ANALYSIS OF THE DATA

3.1. *Surface Brightness Fits*

Radial slices from the surface brightness data were fitted independently using an isothermal model and emissivities taken from Raymond & Smith (1985). In all the fits reported in this paper, the abundances of all elements heavier than helium (C, N, O, Ne, Mg, Si, S, Ca, Fe, and Ni) used in the emissivity code were varied by the same factor, A, while He was kept at its cosmic value. Our results are sensitive primarily to variations in the iron abundance. The emissivity code assumes that the solar number abundance of iron relative to hydrogen is 4×10^{-5}. Our procedure is similar to that followed by Ulmer et al. (1987) but with four differences. First, we extended the range of these fits to the 50′ radius limit of the Spartan 1 data. Second, the present results have greater statistical weight, as they are derived from roughly double the amount of data used by Ulmer et al. (1987). Third, to facilitate comparison with the Spacelab 2 results, we used bins 6′ wide at radii between 0′ and 36′, and grouped the data between 36′ and 50′ into a single bin. Fourth, background was derived using a correction between coincidence and background counts (Fritz et al. 1993; Synder et al. 1990) rather than from data at the end of the scans. The temperature, abundance, and normalization parameters were allowed to vary freely, while the galactic absorption was fixed at the best-fit value of 2.8×10^{21} cm^{-2} obtained by Ulmer et al. (1987). Different values of absorption, including the nominal value of 1.6×10^{21} cm^{-2} taken from H I measurements at the cluster center (Heiles 1975), yielded larger values of χ^2. In the innermost bin, a power-law point source was added to the thermal model to account for a possible nonthermal nuclear source in NGC 1275 (Fabian et al. 1981).

Figure 1 shows the best-fit abundances and 1 σ confidence estimates calculated for a single interesting parameter (Lampton, Margon, & Bowyer 1976; Malina, Lampton, & Bowyer 1976). In the innermost bin we reproduce the result of Ulmer et al. (1987), while values in the next two bins are in statistical agreement with the results for the 6′–20′ bin represented in that work. Fits to the outermost four bins produced

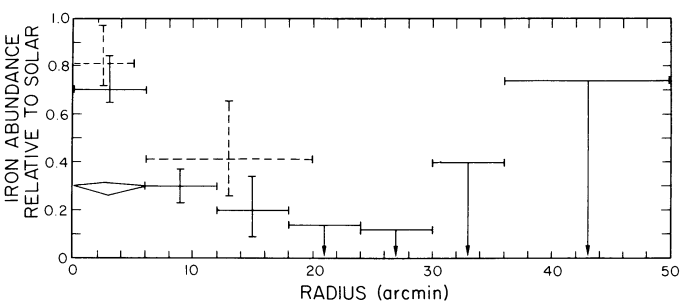

FIG. 1.—Best-fit abundances and 1 σ confidence estimates for a single temperature thermal model fitted to the Spartan 1 data. To account for a nonthermal source at NGC 1275 a power-law point source was added to the thermal model in the innermost bin. Bins between radii of 0′ and 36′ are 6′ in width and the data between 36′ and 50′ have been grouped in a single bin. The dashed symbols are the work of Ulmer et al. (1987), and the uncertainties have been adjusted to 1 σ. The diamond represents a fit where the point source was not included.

only upper limits, and the constraint imposed by the inner two of these bins (18′–30′) strengthens the case for an abundance gradient which was suggested in Ulmer et al. (1987) (χ^2 is acceptable at the 90% confidence level in all four bins). Also, outside the innermost bin, there is excellent agreement between our results in Figure 1 and those of Spacelab 2 (Fig. 2*a* of Ponman et al. 1990). To obtain the most sensitive upper limit possible, we have fitted the data from 18′ to 50′ in a single bin using an isothermal model and obtained a 90% confidence upper limit of 0.15 $A_\odot$ (0.20 $A_\odot$ for 2 σ) to the abundance.

3.2. *Fits Using Three-dimensional Models of the Cluster Structure*

The analysis of the previous section does not provide the most sensitive measure of abundance. First, the abundance is coupled to the temperature and density, which vary both along the slice and along the line of sight. Second, the cluster structure is complicated in the central region, which contains contributions from the point source at NGC 1275 and strong density and temperature gradients associated with the cooling flow. Models of this structure require a large number of free parameters, and these cannot be constrained sufficiently without taking into account emission along the line of sight.

Therefore a second method of analysis was undertaken, in which three-dimensional models were constructed and fitted to the Spartan 1 data. One of the advantages of such models is that they allow for the contribution of emission at large physical radii along the line of sight in the projected inner regions of the cluster. Consequently, in spatial resolved spectral data, more parameters may be constrained with this technique as compared to the more traditional methods described in the previous section. The Perseus cluster is known to have an elliptical structure (Branduardi-Raymont et al. 1981), but the ratio of the minor axis to major axis is 0.83 at radii greater than 20′ (Snyder et al. 1990). Hirayama & Ikeuchi (1978) found that the difference between spherical and elliptical potentials is negligible when this ratio is greater than 0.3, and therefore we have fitted spherically symmetric models to the Spartan 1 data. Also, there is not enough statistical precision in individual scans to permit analysis of nonspherical models.

The procedure assumed radial distributions for the density, temperature, and abundance, all of which contain free parameters. From these distributions the volume emissivity throughout the cluster was calculated using the Raymond & Smith (1985) code, and this was then integrated along the line of sight to produce a two-dimensional map of the photon flux. Then for each radial position of the scanning collimator and at each detector energy channel, a count rate was obtained by integrating the flux over the collimator field of view and then folding the result with the detector response kernel. This model count rate, a function of energy and projected radius, then was compared to the data count-rate. A nonlinear least-squares fitting program calculated χ^2 and adjusted parameters after each iteration until convergence on a best-fit was obtained. The calculation used 21 radial and 13 energy bins, giving a total of 273 points. An investigation of various binning arrangements demonstrated that our results are largely independent of the specific choice of binning. Calculation time for a single set of model parameters was about 300 CPU-seconds on a VAX 6000-320, and a typical fit with all parameters free required 0.5 CPU-days.

A number of models were studied to determine the sensitivity of our results to the particular functional forms chosen for the density, temperature, and abundance. In most models two separate components were used to describe the density and temperature in the cooling flow and in the more extended cluster emission. The density and temperature in these cases were usually required to be continuous across the "critical" radius, also a free parameter, at which the cooling flow and cluster components were joined. Most iron abundance profiles were simple and consisted of a single component, in which abundance either was constant, or was a linear, Gaussian, or "top-hat" function or radius. A point source located at NGC 1275 was included in all models, and different spectral forms for this source were examined. The spatial resolution of H I measurements (Heiles 1975) is coarse compared to that of our X-ray data, and therefore galactic absorption was included as a single value and not allowed to vary during the fit.

Here we present results for our most successful model and only discuss other models when comparing the results to those of other instruments. The model incorporates a cooling flow component in which the density follows a modified King profile and the temperature is a power-law function of radius. The surrounding cluster emission component is similar to the single-component model used by Snyder et al. (1990), having a modified King density profile and a polytropic temperature-density relation. If the polytropic index is restricted to values between 1 (isothermal) and 5/3 (adiabatic), the temperature distribution is constrained either to be flat or to fall with increasing radius. To avoid this restriction, however, we have allowed the index to take on a wide range of values during the fit, even those which would signify a temperature profile which increases with radius.

The results obtained by Synder et al. (1990) were consistent with the intracluster gas being isothermal between radii of 8′ and 50′. As isothermal temperature profiles produce divergent masses, it is desirable to examine the temperature distribution at larger radii. Results from *EXOSAT*, *Tenma*, and *Einstein* observations (Edge 1989; Hughes et al. 1988b) suggest a near-adiabatic falloff in temperature in the Coma cluster beyond a radius of 25′–50′ (1–2 Mpc). Although the center of the Spartan 1 collimator never moved further than 50′ from NGC 1275, the collimator field does sample regions at greater radii. Thus, to place limits on the temperature far from the center of the Perseus cluster, the polytropic exponent in the best-fit model is allowed to change abruptly at a radius of 50′ (1.6 Mpc). This outer region extends to the maximum physical radius sampled during the line of sight and collimator integration, a value of 6 Mpc. A similar model for the temperature distribution in the Coma cluster has been investigated by David, Hughes, & Tucker (1992). The point source at NGC 1275 was given an absorbed power-law spectrum in which the exponent, amplitude, and intrinsic absorption column density are free parameters. As in the previous section, and galactic absorption was fixed at the best-fit value of 2.8×10^{21} cm^{-2} obtained by Ulmer et al. (1987). Finally, the iron abundance was assumed to fall linearly with radius from some peak value at the cluster center.

In Figure 2 we compare the data with the best-fit model for two interesting cases. Figure 2*a* shows a spectrum of the innermost radial bin. Figure 2*b* shows the radial distribution of count rate in the energy bin which contains the iron K-line. In Figure 2*b* the data points at the cluster center oversample the resolution of the stationary Spartan 1 collimator (5′ in the scan direction) by a factor of 5. However, all observations were made by scanning the collimator over the cluster, and in com-

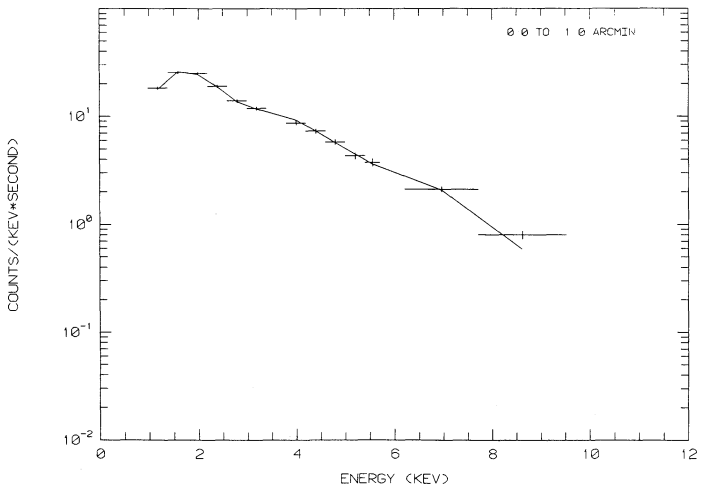

FIG. 2a

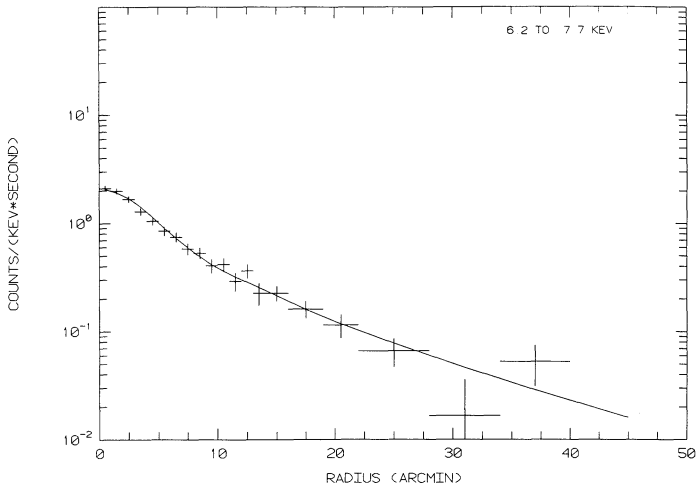

FIG. 2b

FIG. 2.—(*a*) Count-rate spectrum of the best-fit model (*solid line*) and background-subtracted data (*crosses*) in the innermost radial bin (0′–1′). (*b*) Count-rate radial profile of the best-fit model (*solid line*) and background-subtracted data (*crosses*) in the energy bin which contains the iron K-line (6.2–7.7 keV).

bination with the aspect solution, the resulting uncertainties in derived source positions are about 1′ (Snyder et al. 1990). In Table 1 we summarize the free parameters of the model, their best-fit values, and the 90% confidence errors for a single interesting parameter (Lampton et al. 1976; Malina et al. 1976). The minimum value of χ^2 (287.3 for 257 degrees of freedom) is acceptable with confidence greater than 90%. In this paper we will not undertake a detailed examination of the best-fitting model, as our purpose here is to study the distribution of iron in the intracluster gas, and will make only a few short comments:

1. The cooling flow temperature distribution and outer radius (the critical radius) agree well with the results reported by Fabian et al. (1981) for the *Einstein* HRI. However, our density profile is distinctly flatter at radii less than about 2′.

2. The core radius and exponent for the modified King model of the cluster density distribution overlap those derived by Snyder et al. (1990) wherein we compare in detail our results for these parameters with those of the Einstein IPC. The best-fit polytropic exponent, $1.12^{+0.36}_{-0.04}$, is consistent with the finding of Snyder et al. (1990), that the gas is close to being isothermal outside the cooling flow and within 1.6 Mpc.

3. Our observations do not provide a sensitive probe of the gas temperature beyond 1.6 Mpc.

The best fit to the abundance distribution agrees well with the results of analyzing the surface brightness distribution,

TABLE 1

SUMMARY OF THE MODEL FREE PARAMETERS AND THEIR BEST-FIT VALUES[a]

Description	Parameter	Best-Fit Value
Cooling flow density[b]: $\rho\alpha(1 + r^2/a_c^2)^{-Y}$	a_c(Mpc)	$0.20^{+0.11}_{-0.20}$
	Y	$1.89^{+2.02}_{-0.82}$
Cluster density[b]: $\rho\alpha(1 + r^2/a^2)^{-X}$	a (Mpc)	$0.41^{+0.29}_{-0.07}$
	X	$1.09^{+0.36}_{-0.09}$
Cooling flow temperature: $T\alpha r^m$	m	$0.54^{+0.17}_{-0.20}$
Cluster temperature ($r < 1.6$ Mpc): $T\alpha\rho^{n-1}$	n	$1.12^{+0.36}_{-0.04}$
Cluster temperature ($r > 1.6$ Mpc): $T\alpha\rho^{o-1}$	o	$1.42^{+0.65}_{-\ldots}$[c]
Critical radius[d]	r_{cr}(Mpc)	$0.28^{+0.08}_{-0.04}$
Density at the critical radius	$\rho_{cr}(10^{-3}$ cm$^{-3})$	$1.76^{+0.65}_{-0.61}$
Temperature at the critical radius	$T_{cr}(10^7$ K)	$7.95^{+2.23}_{-0.55}$
Abundance[e]: $A = A_0 + (A_1 xr)$	A_0	$0.77^{+0.30}_{-0.38}$
	A_1(Mpc^{-1})	$-1.10^{+0.89}_{-2.24}$
NGC 1275 point source flux[f]: $B \times E^{-\alpha} \times \exp[-\sigma(E)N_H]$	B	$11.24^{+5.45}_{-4.50}$
	α	$2.65^{+0.20}_{-0.45}$
	$N_H(10^{22}$ cm$^{-2})$	$1.49^{+0.69}_{-0.69}$

[a] Galactic absorption fixed at 2.8×10^{21} cm^{-2}. The value of χ^2 was 287.3 for 257 degrees of freedom which is acceptable at the 90% confidence level. In Tables 1 and 2 all errors are quoted at the 90% confidence level for a single interesting parameter.

[b] Density $= \sqrt{\rho_e \rho_p}$; ρ_e and ρ_p are electron and proton densities, respectively. The independent variable, r, has units of Mpc. For the Perseus cluster 1′ $\simeq$ 32 kpc in projection.

[c] Lower limit not constrained.

[d] The critical radius is where the cooling flow and cluster components are joined.

[e] The abundance of all elements heavier than He and relative to solar values.

[f] The amplitude B has units of 10^{-2} photons cm^{-2} s^{-1} keV^{-1}, and the photon energy E is expressed in keV.

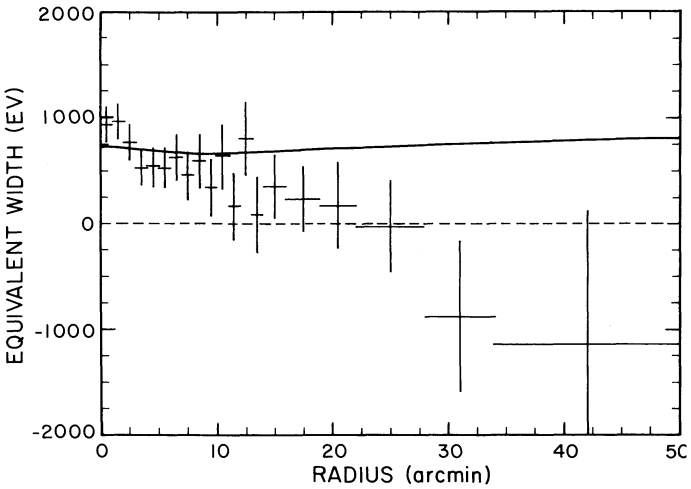

FIG. 3.—Distribution of equivalent width of the iron K-line against radius. The points were obtained by subtracting the best-fit thermal and point source continuum fluxes from the measurements in the iron K-line energy band (6.2–7.7 keV), and then dividing this result by the best-fit thermal continuum flux. The solid line represents the equivalent width which would be produced using the best-fit values for the density and temperature parameters and a constant abundance of 0.4 $A_\odot$.

shown in Figure 1. The iron abundance at the cluster center is $0.77^{+0.30}_{-0.38}\,A_\odot$ (Table 1), and the linear term of the gradient is $-1.10^{+0.89}_{-2.24}\,A_\odot$ Mpc^{-1} (90% confidence for a single interesting parameter in both cases).

The existence of a gradient in the iron abundance is supported by a plot of the equivalent width of the iron K-line against radius, shown in Figure 3. The points in this figure have been obtained by subtracting the best-fit thermal and point source continuum fluxes from the measurements in the iron K-line energy band (6.2–7.7 keV), and then dividing this result by the best-fit thermal continuum flux. In Figure 3 we also show the equivalent width which would be produced using the best-fit values for the density and temperature parameters and a constant abundance of 0.4 $A_\odot$. This line is flatter than the observed equivalent width and is significantly higher than the data in the outer regions of the cluster. Given the approximately isothermal nature of the gas outside of the cooling flow, these results imply that again the abundance is falling to low values at a radius of approximately 20′. A model with constant equivalent width fitted to these data may be rejected with 90% confidence, and the addition of a linear term is highly significant, reducing χ^2 from 26.1 to 10.9 (19 degrees of freedom). A linear fit is acceptable at a confidence level greater than 90% and yields a peak equivalent width of 839 ± 70 eV and a gradient of -38 ± 7 eV arcmin^{-1}.

As a consequence of these results we have made a careful analysis of the limits to the rate of falloff of abundance with radius. In Table 1 we quote 90% confidence limits for a single interesting parameter ($p = 1$). However, the central abundance and gradient parameters are coupled, and a rigorous examination requires the limits be calculated jointly for two interesting parameters ($p = 2$) as described by Malina et al. (1976) and Lampton et al. (1976). The results are shown in Figure 4*a*. When projected on either axis, the joint 68% confidence (1 σ) limits are in good agreement with the 90% confidence limits for a single interesting parameter. This result is expected as $\chi^2_p(\alpha)$, where α is the confidence level, is 2.3 for $p = 2$ ($\alpha = 0.68$) and 2.71 for $p = 1$ ($\alpha = 0.90$). However, for $p = 2$ and $\alpha = 0.90$ confidence, the value of $\chi^2_p(\alpha)$ is 4.61. In Figure 4*a* the χ^2 surface flattens out at steep values of the gradient so that the 90% confidence limit is not constrained. Thus, when the central abundance is considered jointly with the gradient, the Spartan 1 data cannot reject high central abundances. However, this result is caused by the large number of free model parameters, particularly in the central region containing the cooling flow and the point source, which allow large excursions from the best-fit abundance without increasing χ^2 and allow parameter

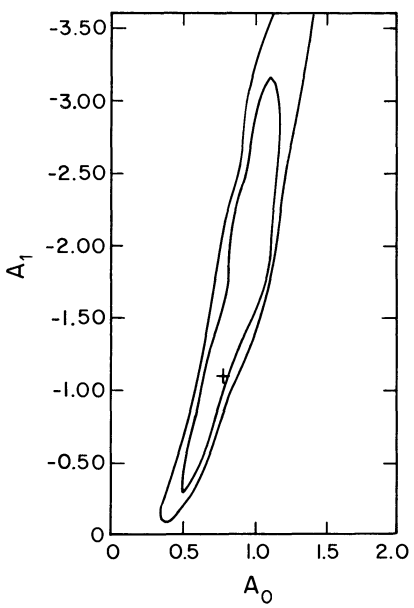

FIG. 4*a*

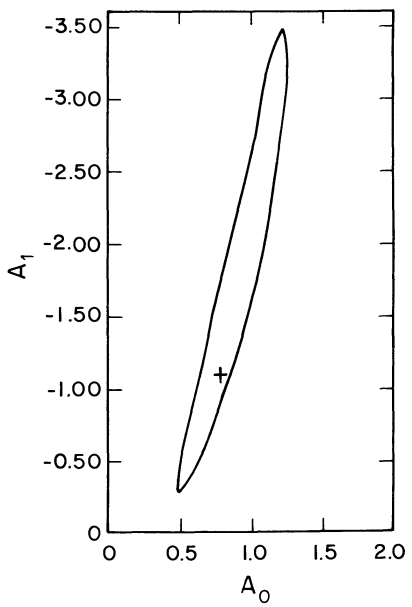

FIG. 4*b*

FIG. 4.—(*a*) Joint 1 σ and 90% confidence limits for the central abundance and gradient model parameters (Table 1). The best-fit is represented by a plus sign. (*b*) Same as (*a*) but the cooling flow temperature exponent and density core radius and exponent were fixed at their best-fit values. Only the 90% confidence contour is shown.

values on the 90%-contour to reach unphysical situations. As we are interested primarily in setting limits to the abundance distribution outside of this central region, we have recalculated the 90% confidence limits for two interesting parameters, this time fixing the cooling flow temperature exponent, density core radius, and density exponent at their best-fit values. The results is shown in Figure 4*b*.

In Figure 5*a* we have transformed the resulting 90% confidence limits in Figure 4*b* into an envelope of allowed abundance distributions. Figure 5*b* is a similar plot of 90% confidence limits using a Gaussian abundance distribution (cooling flow parameters fixed). The close agreement between envelopes for these two different functional forms supports the case for a true abundance gradient and suggests that the Spartan 1 results are fairly independent of the abundance model as long as it provides for a gradient. Note that the results in Figure 5 do not allow a constant abundance at 90% confidence. The limits to the radius at which the abundance in Figure 5*a* goes to zero are 0.35–1.72 Mpc (11′–54′ in projection), and this envelope can be used to place limits on models of cluster structure and evolution.

3.3. *Comparison to Other Observations*

In Snyder et al. (1990) we used a polytropic temperature-density relation to fit the radial distribution of the measured broad-band surface brightness and hardness ratio data over the range 8′–50′. We found that the polytropic index was consistent with an isothermal distribution and that the result disagreed with the value derived from *HEAO 1* A-2 data (Henricksen 1985). This difference was discussed in Synder et al. (1990), where we argued that the A-2 instrument sampled a much larger area around the cluster center, so that the derived polytropic index may be some average over an isothermal inner region and an adiabatic outer one. However, when the abundance gradient is included, there is a modest change in the Spartan 1 result. The best-fit polytropic index for radii less than 1.6 Mpc is now $1.12^{+0.36}_{-0.04}$, which implies a slight but statistically significant decrease in temperature with radius (Table 1). Thus a measure of agreement with the *HEAO 1* A-2 result is obtained with the caveat that their analysis did not provide for an abundance gradient.

The University of Birmingham Spacelab 2 instrument observed the Perseus cluster about 1 month after Spartan 1, and analyses very similar to ours have been performed (Ponman et al. 1990; Eyles et al. 1991). Table 2 is a summary and comparison of best-fit values and 90% confidence limits obtained from the Spartan 1 and Spacelab 2 analyses. Qualitatively, their abundance distribution agrees with ours in that a gradient is required to obtain an acceptable fit to their data, and except for the innermost bin, the Spartan 1 abundances produced from fits to the surface brightness distribution (Fig. 1) are in excellent agreement with the Spacelab 2 results (Fig. 2*a* of Ponman et al. 1990). For Spacelab 2 a constant abundance model may be rejected with greater than 99% confidence in fits to data which include the central region of the cluster, and a 90% confidence upper limit of 0.1 $A_\odot$ may be set to the abundance at radii larger than 0.8 Mpc (modified top-hat model). For Spartan 1 constant abundance models with different abundances were fitted to the data between 0′ and 50′, and all could be rejected (95% confidence). Also, a constant abundance model was fitted just to the data at radii greater than 0.7 Mpc (22′–50′), and an upper limit of 0.2 $A_\odot$ (90% confidence) was obtained. However, the results in Table 2 also reveal a significant discrepancy between the two experiments, in that the Spacelab 2 central abundance is consistently higher than the Spartan 1 value and its gradient is steeper. Knowledge of the abundance distribution of heavy elements is an important factor in understanding cluster structure and evolution, and therefore strong efforts were made by NRL and the University of Birmingham group to understand this discrepancy. Here we relate three efforts and consider explanations for the difference.

As the cluster structure in the central region is complicated by the cooling flow and point source, we represented the fit using data from only the outer regions of the cluster. Using

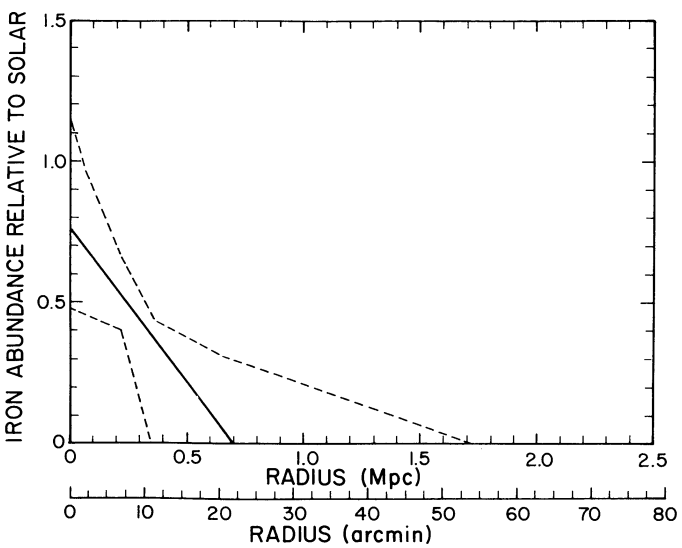

FIG. 5*a*

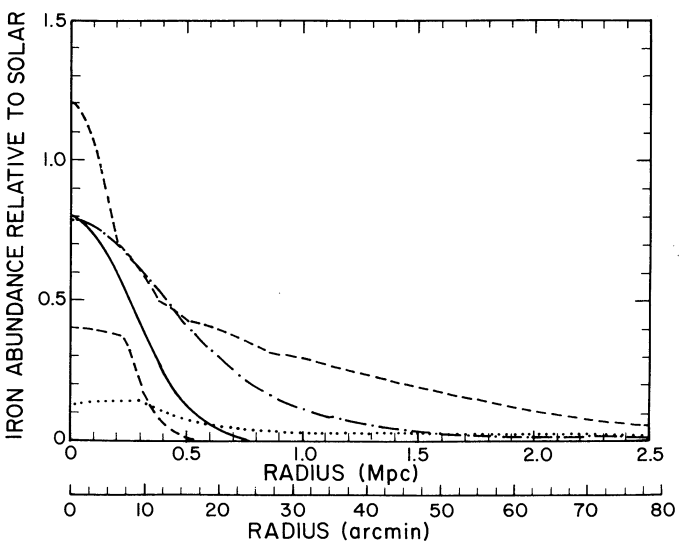

FIG. 5*b*

FIG. 5.—(*a*) Envelope of allowed abundance distributions (*dashed lines*) determined from the confidence contour shown in Fig. 4*b*. The best-fit is represented by a solid line. (*b*) Same as (*a*) but for a Gaussian abundance distribution. The dotted line was calculated for a theoretical model with an assumed constant gas mass-loss rate per galaxy of 10^{-11} yr^{-1} and the dot-dashed line was calculated for a model in which the galaxy mass-loss rate was proportional to the gas density.

TABLE 2

COMPARISON OF SPARTAN 1 AND SPACELAB 2 BEST-FIT ABUNDANCE DISTRIBUTIONS

Linear $A_0 + (A_1 \times r)$	Gaussian $A_0 \times \exp[-0.5 \times (r/A_s)^2]$	Top Hat A_0 for $r < r_0$, 0 for $r \geq r_0$
SPARTAN 1[a]		
$\chi^2 = 287.3$	$\chi^2 = 288.2$	$\chi^2 = 287.7$
$A_0 = 0.77\ +0.30\ -0.38$	$A_0 = 0.79\ +0.31\ -0.35$	$A_0 = 0.57\ +0.37\ -0.20$
$A_1 = -1.10\ +0.89\ -2.24$	$A_s = 0.26\ +0.03\ -0.14$	$r_0 = 0.39\ +0.12\ -0.13$
SPACELAB 2[b]		
$\chi^2 = 23445$	$\chi^2 = 23441$	$\chi^2 = 23427$
$A_0 = 2.32$[c]	$A_0 = 2.19\ +0.16\ -0.16$	$A_0 = 1.76\ +0.07\ -0.12$
$A_1 = -6.25$[c]	$A_s = 0.17\ +0.03\ -0.03$	$r_0 = 0.30\ +0.02\ -0.02$

[a] The fits had 257 degrees of freedom. A constant abundance could be rejected with greater than 95% confidence. The scale parameters (A_1^{-1}, A_s, and r_0) have units of Mpc.

[b] The fits had 23,213 degrees of freedom. A constant abundance could be rejected with greater than 99% confidence. After reexamination of systematic errors, Ponman et al. 1991 revised the value of A_0 from 2.09 (Ponman et al. 1990) down to 1.76 for the top-hat model. Values for the Gaussian model have been revised already (Eyles et al. 1991). As a similar reduction is expected for the linear model (Ponman 1990), we have scaled A_0 (2.75, Poman 1990) down to the value given here.

[c] Errors not available for this model.

data obtained at radii between 8′ and 50′, when the point source and the intense core of the cooling flow (radius $< 3'$) are never in the collimator's field for view, acceptable fits were obtained in which the central abundance, deduce by extrapolation, was $1.0 \pm 0.9\ A_\odot$, and the gradient was $-1.3^{+1.3}_{-2.2}\ A_\odot$ Mpc^{-1} (90% confidence). Although these results cannot rule out a constant abundance, both the central abundance and gradient were consistent with the values obtained from fits to data between 0′ and 50′. These results are also consistent with Snyder et al. (1990) who obtained acceptable fits for the same range of data and an assumed constant abundance of $0.5\ A_\odot$. Likewise, Ponman (1990) fitted the outer region (radius $> 8'$) of the Spacelab 2 data and obtained a similar result, namely an acceptable fit yielding a slight increase in their central abundance. Therefore, we can conclude that for both instruments the abundance distribution deduced by analyzing this outer region is consistent with that obtained for the whole cluster. This implied that the discrepancy between the two results was not sensitive to the assumptions made in deriving the flux from NGC 1275 and the surrounding cooling flow. Nevertheless, because the density, temperature, abundance, and point source parameters are coupled, both groups examined the sensitivity of their results to the functional forms chosen for the density and temperature.

First, the Spartan 1 data were fitted using the Spacelab 2 model. This model differs from ours in the use of power-law distributions for the density in the cooling flow region, and for the temperature in the region outside the cooling flow, and in the decision to fix all parameters of the cooling flow to match the HRI temperature deconvolution ($K = 3$ curve in Fig. 5 of Fabian et al. 1981) and either the IPC density profile (Fig. 2 of Branduardi-Raymont et al. 1985) or the HRI density profile ($K = 3$ curve in Fig. 6 of Fabian et al. 1981). (Table 2 of Eyles et al. 1991 shows the effect on the Spacelab 2 results of fixing different values for some of the model parameters.) Our standard fitting procedure was to let all model parameters vary freely. We fit the Spacelab 2 model to the Spartan 1 data under three assumptions: (1) all parameters were free, (2) all parameters were fixed at the Spacelab 2 best-fit values (Ponman et al. 1990; Eyles et al. 1991), and (3) only cooling flow parameters were fixed. In all cases we could reject the fit with greater than 95% confidence, and this result was obtained regardless of the function form of the abundance distribution or the value of galactic absorption. The best-fit central abundance for a Gaussian abundance distribution in cases 1 and 3 was less than $0.7\ A_\odot$, and case 2 with its higher central abundance ($2.2\ A_\odot$, Gaussian abundance model; see Table 2 and Eyles et al. 1991) yielded the worst value of χ^2. These results confirm that the Spartan 1 data require a central abundance lower than the Spacelab 2 data regardless of the form of the density and temperature distributions.

Second, both the deconvolved IPC density (Fig. 2 of Branduardi-Raymont et al. 1985) and the HRI density ($K = 3$ curve of Fig. 6 in Fabian et al. 1981) show some curvature (flattening) at radii less than $\sim 2'$, and this is not well represented by the power-law distribution of the Spacelab 2 model. The Spartan 1 model has a modified King distribution for the cool flow density which can accommodate curvature better. Therefore we refit the Spartan 1 model with cooling flow parameters fixed to match visually the HRI temperature ($K = 3$ curve) and either the IPC or HRI density ($K = 3$ curve) profiles. However, both these fits could be rejected with greater than 99% confidence (χ^2 is 349.3 and 236.5 with 265 degrees of freedom for the IPC and HRI density models, respectively).

Third, Ponman (1990) has fitted the Spacelab 2 data with the Spartan 1 model. With all parameters fixed at our best-fit values, they obtained an unacceptable value of χ^2. When the abundance is allowed to vary, the fit becomes acceptable, but the central abundance climbs to about $3\ A_\odot$.

What then is the correct density distribution in the cooling flow? The spatial resolution of the *Einstein* imaging instruments is much better than that of both the Spartan 1 and Spacelab 2 instruments, and as the imaging instruments are sensitive primarily to the density, it should be well defined by them. However, the HRI (Fig. 6 of Fabian et al. 1981) and IPC density (Fig. 2 of Branduardi-Raymont et al. 1985) deconvolutions differ by as much as a factor of 2 at a radius of 600″. Moreover, the HRI results were calculated for an assumed constant abundance of $0.5\ A_\odot$ (Branduardi-Raymont et al. 1985 do not state what abundance distribution was used for the IPC density deconvolution). As both the Spartan 1 and Spacelab 2 results demonstrate an abundance gradient, it is not

clear what effect this might have on the HRI or IPC deconvolutions.

The point source at NGC 1275 is a similar cause for concern as the abundance and point source parameters are coupled. Although the Spartan 1 collimator could not spatially resolve the point source emission, a point source was required in our model to obtain an acceptable fit to the data. However, neither the Spartan 1 nor the Spacelab 2 instrument is capable of determining all three point source parameters well. The high energy response of the Spacelab 2 detectors constrained the power-law index well ($\alpha = 2.4 \pm 0.4$), and the Spartan 1 result (Table 1 and Ulmer et al. 1987) is in agreement with their results. However, the amplitude derived from the Spacelab 2 data is somewhat sensitive to the assumed abundance distribution. Eyles et al. (1991) obtained a value of $7.6^{+2.3}_{-1.7} \times 10^{-2}$ photons cm^{-2} s^{-1} keV^{-1} with a Gaussian radial abundance distribution, and Ponman et al. (1990) derived $4.1^{+1.0}_{-0.8} \times 10^{-2}$ photons cm^{-2} s^{-1} keV^{-1} with a top-hat radial abundance distribution (90% confidence, as obtained from converting the 1 σ errors in Ponman et al. 1990). The Spartan 1 best-fit amplitude was relatively insensitive to the form of the abundance distribution, and the value in Table 1 ($11.24^{+5.45}_{-4.50} \times 10^{-2}$ photons cm^{-2} s^{-1} keV^{-1}) agrees well with the result derived from surface brightness fits ($11.0 \pm 3.0 \times 10^{-2}$ photons cm^{-2} s^{-1} keV^{-1}) by Ulmer et al. (1987). The Spacelab 2 results were derived for an assumed galactic absorption of 1.4×10^{21} cm^{-2} and total absorption at NGC 1275 of 4.3×10^{21} cm^{-2}, as derived from reddening measurements of NGC 1275 (Gorenstein et al. 1978). However, their results were insensitive to these choices (Poman 1990). The Spartan 1 low-energy response was used to place limits on the absorption instrinsic to the point source at NGC 1275, and the best-fit result (Table 1) is a factor of 5 times higher than that indicated by reddening measurements.

To determine what effect the point source parameters and the galactic column density might have on our derived abundance results, we conducted a series of fits to obtain a map of χ^2 and the abundance parameters (Table 1) in the space (B, α, $N_{\rm H}$, $N_{\rm Hgal}$). With all other parameters free (density and temperature), the abundance parameters remained in agreement with the values given in Table 1, as long as the point source parameters were fixed at values within the single-parameter 90% confidence intervals given in Table 1. When the point source parameters exceeded these intervals, the abundance parameters could fall outside the confidence intervals given in Table 1. However, in all such cases, the fit could be rejected with greater than 95% confidence. This result is not surprising as the density and temperature parameters can compensate to some extent for changes in the point source continuum. However, our derived abundance is driven primarily by the strength of the iron K-line complex and is therefore not as strongly coupled as density and temperature to the point source. Therefore we repeated the mapping exercise, this time with the density and temperature parameters fixed at their best-fit values, but the results of this investigation were essentially the same as the case where all parameters were free. We conclude that coupling between point source and abundance parameters cannot account for the abundance gradient.

As discussed, the Spartan 1 data could reject models (95% confidence) with a galactic absorption column of 1.6×10^{21} cm^{-2}, a value taken from H I measurements at the cluster center (Heiles 1975). Only models with galactic column densities between 2.28 and 5.12×10^{21} cm^{-2} were acceptable, in good agreement with the best-fit value of 2.8×10^{21} cm^{-2} obtained by Ulmer et al. (1987). This value is also in agreement with that obtained from spectral measurements made by the *Einstein* SSS, but White et al. (1991) have attributed this excess absorption to cold X-ray absorption clouds in the cooling flow. However, the SSS observations were confined to the center of the cluster ($r < 3'$). If a similar analysis is performed on the Spartan 1 data which exclude the central region ($r > 8'$), a column density of 1.6×10^{21} cm^{-2} may be rejected with 95% confidence. In all cases, though, we found that our derived abundance values were not sensitive to the chosen value of galactic absorption.

Finally, the different point source amplitudes obtained by the Spacelab 2 and Spartan 1 observations suggest variability in the nucleus of NGC 1275. Although Primini et al. (1981) did not detect variability on 6 month time scales in the *HEAO 1* A-4 data, Rothschild et al. (1981) found evidence for variability on time scales of years by comparing hard X-ray fluxes measured by *OSO 7* (1972), a balloon experiment (1974), and *HEAO 1* A-4 (1978); however, these experiments could not resolve spatially the point source component. The two *Einstein* HRI observations of NGC 1275 are separated by approximately 1 year. We copied the photon event files from the archive (sequence numbers 285 and 287) and used PROS to determine the flux in a circle of 8″ radius centered on NGC 1275. The HRI resolution element has a radius of 4″, and the point source is not resolved. Emission from the cooling flow, the extended cluster component, and the background was calculated in an annulus with inner and outer radii of 8″ and 24″, respectively. Figure 5 of Branduardi-Raymont et al. (1981) shows a model of the HRI cluster surface brightness with the point source subtracted. This profile is flat at radii less than about 30″. Also, the variation in background over such a small source region is minimal. Thus, to obtain an estimate of the point source flux, we have subtracted the annulus emission from the emission in the circular region centered on NGC 1275. The result is 0.230 ± 0.004 counts s^{-1} for the first observation and 0.269 ± 0.007 counts s^{-1} for the second observation, a statistically significant increase of 17%. As the HRI had no spectral resolution, it was impossible to determine which of the three parameters of an assumed power-law spectrum varied. Hard X-ray spectra in Seyfert 1 sources tend to soften as the flux increases, and this has been modeled by variations in the intrinsic column density, in the power-law index, or in the use of a two-component model spectrum (Morini et al. 1986).

The Spartan 1 and Spacelab 2 observations were separated in time by about 1 month. However, Mushotzky et al. (1980) and Piro et al. (1988) have found that variability is a common phenomena in Seyfert 1 galaxies on time scales as short as hours. In both the Spartan 1 and Spacelab 2 analyses the point source results were derived from fits to the data, and therefore any variability in the continuum caused by NGC 1275 should not affect the abundance parameters, if properly accounted for in the point source model. On the other hand, a change in the central abundance might be caused by Seyfert line emission from NGC 1275. To investigate this, Ponman et al. (1990) added a point source iron line at 6.4 keV to the continuum. Their results do allow a significant contribution to the total iron line emission from the source, while not changing the radius at which the abundance drops to zero (top-hat abundance model of Table 2). We find that the addition of a point source iron line at 6.4 keV does not reduce χ^2 significantly, and

we derive a 90% confidence upper limit of $\sim 1 \times 10^{-4}$ photons cm^{-2} s^{-1} keV^{-1} in the line. Thus, we conclude that line emission at 6.4 keV from NGC 1275 could explain the discrepancy in the central abundance between the Spartan 1 and Spacelab 2 results if it were variable in the sense that the line emission was on during the Spacelab 2 observation but off during the Spartan 1 observation. Thus, the Spartan 1 result would represent the true abundance distribution of iron in the intracluster gas.

To summarize, we find that except for the crucial issue of the iron abundance at the cluster center, there is broad agreement between the Spartan 1 and Spacelab 2 results. Even with different models the best-fit polytropic indices from both instruments (Table 1 and Eyles et al. 1991) indicate a shallow temperature gradient in the cluster emission, and the densities are always within 30% of each other out of 50′. Although the Spartan 1 and Spacelab 2 central abundances and gradients differ, the radii at which the abundance drops to a small value, for example, in the case of the top-hat abundance distribution (Table 2), are in statistical agreement. The disagreement in the central abundance might be caused by variable iron-line emission (6.4 keV) in the nucleus of NGC 1275.

In the SSS observations of the Perseus cluster (Mushotzky et al. 1981), L-lines of iron at 1 keV and Si and S lines at higher energies were identified in the spectrum. Fits of a two-thermal component model yielded an iron abundance of 0.35 ± 0.02 $A_\odot$ (90% confidence) after adjustment to a value of 4×10^{-5} for the solar number density of iron relative to hydrogen. This result disagrees with the Spartan 1 result in Figure 5 and, in conjunction with the abundances derived from broad-field measurements, is consistent with there being no radial abundance gradient in the cluster. However, the SSS had no high-energy sensitivity and no spatial resolution. No point source contribution was modeled, and consequently the abundance may be underestimated. The derived abundances for the Si and S lines were 0.9 ± 0.5 and 1.4 ± 0.4 $A_\odot$ (90% confidence), respectively. It is interesting that the lighter elements have abundances relative to the solar value that are greater than iron, and a similar result has been found for oxygen by the high-resolution *Einstein* FPCS (Canizares, Markert, & Donahue 1988).

More recently, the BBXRT instrument made several observations of the Perseus cluster with good spectral resolution, but with limited spatial resolution. A preliminary analysis (Petre 1991) has been performed of one field, in which the BBXRT was pointed approximately at the cluster center. A single thermal source model provides an acceptable fit to the data in the central segment of the detector (radius = 2.′25) with a best fit abundance of 0.5 ± 0.1 $A_\odot$. A point source contribution was not included in this fit because NGC 1275 was located on an insensitive area of the detector which divides the central segment from the segmented outer annulus (Mushotzky 1992). The telescope point spread function is narrow so that only 20% of the possible point source photons may be scattered into adjacent detector segments, and the addition of a point source, attenuated by this amount, did not reduce χ^2 significantly. Data in the annular segments of this field and in another field which is centered several arcminutes to the southwest of NGC 1275 have been analyzed now in a similar manner, and the derived abundances are 0.5 ± 0.2 $A_\odot$ at a radius of 6′ and 0.5 ± 0.5 $A_\odot$ at a radius of 12′ (Mushotzky 1992). These results provide no evidence for a gradient and formally disagree with the results obtained from the Spacelab 2 instrument. However, they cannot rule out a gradient of the size reported here. In addition, the BBXRT results were derived from spectral fits of a single component model which did not take the cooling flow into account. Therefore further analysis of the BBXRT data is required before a critical comparison with the Spartan 1 results is possible.

The *Ginga* satellite also has made several observations of different regions within the Perseus cluster (Allen et al. 1992). The field of view of the collimator for the Large Area Counter is 1° × 2° FWHM, and pointings were made with the collimator center offset from the cluster center in 0.°75 steps along a position angle of 170°, where the long axis of the collimator was kept perpendicular to the line connecting the collimator and cluster centers. A single component thermal model was fitted to the data at offsets of 0.°75, 1.°5, and 3.°0, whereas at the cluster center and additional cooling flow component was required for an acceptable fit. Abundances of 0.41 ± 0.02 and 0.37 ± 0.05 $A_\odot$ were obtained from data taken at offsets of 0° and 0.°75, respectively, while data taken at offsets of 1.°5 and 3.°0 allow abundances between 0 and 0.5 $A_\odot$ (90% confidence; see Table 1 and Fig. 3*b* of Allen et al. 1992). Allen et al. (1992) use a value of 3.16×10^{-5} for the solar number abundance of iron relative to hydrogen. If we adjust the Spartan 1 results to this value, then the abundance for the *Ginga* observation which was pointed at the cluster center lies beneath the lower limit of the 90% confidence envelopes shown in Figure 5, while the *Ginga* abundance result for the 0.°75 offset observation lies above these envelopes.

A number of factors should be considered in comparing the Spartan 1 and *Ginga* results. First, the Spartan 1 results in Figure 5 were derived using a model which takes into account emission along the line of sight and the spatial resolution provided by a narrow moving collimator. The *Ginga* instrument has a broad field of view, which tends to blur out the presence of gradients, and no attempt has been made to model the cluster in three dimensions. Second, Allen et al. (1992) claim that the point source contribution (2–10 keV band) has been overestimated in experiments which did not include a cooling flow component in the analysis or where the cooling flow was modeled incorrectly. They found that the addition of a point source at NGC 1275 did not improve the value of χ^2 by a significant amount. In our work we have included a cooling flow component and a point source, and investigated models where the cooling flow component was either free or was fixed to match the *Einstein* results. In all cases the inclusion of a point source was found to reduce χ^2 significantly. Finally, the outermost *Ginga* observations are hampered by low count rates and place no strong constraints on the existence of an abundance gradient.

4. DISCUSSION

4.1. *Cluster Structure and Evolution*

The observation of iron K-line emission in the intracluster gas implies that some gas has been expelled or stripped from galaxies. The Spartan 1 abundance results (Fig. 5, Table 1) indicate that the fraction of intracluster gas that has been ejected from galaxies increases toward the cluster center. However, David et al. (1990) have shown that the ratio of gas to stellar mass averaged over five core radii is greater than three in rich clusters, and therefore the gas is mainly primordial. Nevertheless, the spatial distribution of the ratio of primordial to ejected gas in an important diagnostic of the

cluster's evolutionary history. There are a number of mechanisms for extracting gas from galaxies, for example, ram pressure ablation, galactic winds, thermal evaporation, and stripping by galaxy collisions, and much theoretical effort has been devoted to understanding these processes. Unfortunately, comparison of observations with theoretical models is not straightforward, for a comprehensive model should consider not only all these mechanisms, but in addition various processes which occur after extraction, such as evolution of the cluster as a whole, mixing of expelled and primordial gas, and settling of iron in the core by diffusion. These processes may be in opposition, some leading to abundance gradients and others working to reduce gradients. Sarzazin (1986) has provided an excellent review of both extraction mechanisms and evolutionary processes within clusters. We consider here a number of theoretical models which predict the cluster abundance distribution, and compare them with our data.

Our arguments below assume that the abundance of the ejected galactic gas is solar at all times, implying that galaxies retain no primordial component and that supernova enrichment leads to solar abundances of iron in the galactic gas. White (1991) argues qualitatively that galactic winds should have approximately solar abundances. However, David, Forman, & Jones (1991) have shown that the metallicity of such winds varies with time and depends strongly upon the initial stellar mass function within cluster galaxies. They find that a flat function is required to supply sufficient iron to account for the radially averaged observed abundances of clusters.

4.1.1. *Gas-Removal Processes*

Gunn & Gott (1972) were among the first to suggest that cluster spiral galaxies could be stripped by ram pressure because of their high velocity through the intracluster medium. This mechanism provides a straightforward explanation for an abundance gradient, as stripping is very efficient in the core where both the gas density and galaxy velocities are high. They predicted the onset of stripping at a density of $\sim 5 \times 10^{-4}$ cm^{-3}, in good agreement with the Spartan 1 best-fit model, in which the density falls to this value at a radius, ~ 0.8 Mpc (25′), where the abundance is becoming small. The analysis of Gunn & Gott (1972) has been followed by hydrodynamic calculations of ram-pressure stripping of spherical galaxies by Lea & De Young (1976), Gisler (1976), Nepveu (1981a, b), Takeda, Nulsen, & Fabian (1984), and Gaetz, Salpeter, & Shaviv (1987). These studies have shown that ram pressure may be efficient at densities as low as 10^{-4} cm^{-3}, which corresponds with a radius of about 1.7 Mpc in the Spartan 1 best-fit model, consistent with the limits of the abundance envelopes shown in Figure 5.

The Spartan 1 results in Figure 5 do not constrain the abundance distribution sufficiently to check the validity of detailed stripping models (e.g., Gaetz et al. 1987). However, we have compared a number of simpler stripping models to our results. In each case this was done by first using the best-fit abundance distribution to subtract the ejected component from the total gas density (best-fit in Table 1) and thereby produce the density distribution of the primordial gas component. Then a theoretical density distribution of ejected gas was calculated by multiplying the density distribution of galaxies by a stripping function. For the galaxies, we have assumed a King model with a core radius of 0.34 Mpc and a normalization of 1850 galaxies deg^{-3} (Kent & Sargent 1983). This normalization converts to a value of 5.3×10^{-5} $M_\odot$ pc^{-3}. The gas and galaxy distributions as well as the stripping functions were assumed to be constant over a Hubble time (no evolution). Under the final assumption that the ejected gas has solar abundance, the predicted model abundance was calculated as the ratio of the ejected gas density to the sum of the ejected and primordial gas densities. This result was in turn compared with the measured 90% confidence abundance envelopes shown in Figure 5. As our stripping functions have no radial cutoff we have chosen to display selected models only on Figure 5*b*, the Gaussian abundance envelope.

Three unitless stripping functions, $f(r)$, were examined. the first of these, chosen for simplicity, assumes that the stripping rate is constant throughout the cluster, $f(r) = \alpha/H_0$, where α is the unit mass-loss rate per galaxy. Gisler (1979) has shown that the value of α depends upon the replenishment rate of gas within a galaxy, and values between 10^{-11} yr^{-1} and 3×10^{-11} yr^{-1} are reasonable. Huchtmeier, Tammann, & Wendker (1975) have measured mass-loss rates of 10^{-11} yr^{-1} in nearby elliptical galaxies, and in Figure 5*b* (dotted line) we show the predicted abundance profile for a constant stripping function with this mass-loss rate. This result seriously underestimates the abundance at distances less than one core radius from the cluster center, and mass-loss rates near the limit of 3×10^{-11} yr^{-1} overestimate the abundance at radii greater than 0.5 Mpc. We conclude that constant mass-loss stripping models are not consistent with our data, and some enhancement of the stripping rate at low radii is required.

We have considered two other stripping functions, an inverse-*r* relation and a function where the stripping rate per galaxy is proportional to the gas density, so that the unit volume stripping rate goes as the product of the gas and galaxy densities (Hughes 1991). As they produce similar results we discuss only the latter, $f(r) = (\alpha/H_0) \times [\rho(r)/\rho_{1.7}]$, where $\rho(r)$ is the gas density distribution and $\rho_{1.7}$ is the gas density at a radius of 1.7 Mpc. This choice of normalization is somewhat arbitrary, but allows us to create abundance profiles which fall within the 90% confidence envelope of Figure 5*b* for values of the mass-loss rate α which do not exceed 3×10^{-11} yr^{-1}. This stripping function includes assumptions that there is little variation in galaxy cross sections and that galaxy velocities are roughly constant in the core. We show the result for this model in Figure 5*b* (dot-dashed line), again for a mass-loss rate of 10^{-11} yr^{-1}. As a consequence of the enhanced stripping at small radii, the predicted abundance is in reasonable agreement with our mass confidence envelope.

Galactic winds provide a second process which may enrich the intracluster medium with heavy elements. Originally proposed by Mathews & Baker (1971) to explain the absence of gas within ellipticals and the existence of nonthermal radio halos, this mechanism has been investigated extensively by another authors. Ikeuchi (1977), De Young (1978), and David et al. (1991) found that an early explosive era of supernovae may produce galactic winds which enrich the intracluster medium, leading to the observed radially averaged abundances in clusters. However, David et al. (1991) finds that the resulting iron abundance is a sensitive function of the initial stellar mass function of cluster galaxies, and also that galactic winds may continue to expel gas throughout the lifetime of the cluster in low-luminosity elliptical galaxies. The question of whether a galactic wind model can produce an abundance gradient is more complicated. If the energy within the winds is sufficient to thoroughly mix the ejected and primordial components, then a

constant mass-loss function as discussed above is a reasonable model. The largest mass lost in any of De Young's models in $\sim 6 \times 10^{11}\ M_\odot$ (Table 2 of that work) which correspond to an α of about $3 \times 10^{-10}\ \mathrm{yr}^{-1}$ when averaged over a Hubble time. This would lead to a predicted abundance distribution that agreed only in the core region with the Spartan 1 measured confidence envelope, but overestimated the abundance at radii greater than about 1 Mpc.

Gunn & Gott (1972) suggested another gas removal mechanism, whereby heat conducted from the intracluster gas may warm and evaporate the relatively cooler galactic gas. Cowie & Songaila (1977) predicted evaporation rates as a function of local density and temperature for a single spiral galaxy of disk radius 15 kpc and thickness 200 pc. Their predictions exclude densities greater than 10^{-3}, typical of the cooling flow of the Perseus cluster, and their results (Fig. 1 of Cowie & Songaila 1977) are divided into three regions. In the first region, densities are greater than $10^{-5}\ \mathrm{cm}^{-3}$ but temperatures are lower than 10^7 K, and consequently intergalactic material condenses onto the galaxy. At higher temperatures or lower densities evaporation can occur, and the mass loss depends upon temperature only. Finally, in the third region, the temperature reaches values where the evaporation rate is limited by the number of electrons available to transport the heat at the interface between the galaxy and the intracluster medium, and mass-loss rate has roughly equal dependence on temperature and density.

We have compared our results with these predictions and find that our best-fit model lies entirely in the third region of inhibited evaporation. Evaporation rates are large, ranging from $0.5\ M_\odot\ \mathrm{yr}^{-1}$ at 4.25 Mpc to $31\ M_\odot\ \mathrm{yr}^{-1}$ at 0.5 Mpc. When we plot these rates as a function of radius, the profile is roughly exponential, $\dot{M} \simeq 40 \times \exp(-1.1r)\ M_\odot\ \mathrm{yr}^{-1}$ galaxy^{-1}, for $r > 0.5$ Mpc. To determine whether this result could produce an abundance gradient we convolved this profile with a King density model for the galaxy distribution as was done for the ram-pressure stripping models. We found that the resulting predicted gradient was in good agreement with the abundance envelopes of Figure 5, which indicates that thermal evaporation by itself might account for the observed abundance gradient. This agreement could be fortuitous, however, as heat conduction is a strong function of the magnetic field structure around the cluster galaxies. Unfortunately, detailed knowledge of the magnetic field structure, which is required to determine accurately the contribution of thermal evaporation to the observed abundance gradient, does not yet exist.

4.1.2. *Evolution of the Intracluster Gas*

The major conclusion of the previous section is that some mechanism is required to enhance the mass-loss rate at low radii, possibly ram-pressure stripping or thermal evaporation. However, the discussion there did not include possible evolution in the gas and galaxy distributions. In the literature less attention has been given to evolution of the intracluster medium than to gas extraction mechanisms. If evolution is important the conclusions derived from limits set by the abundance distribution should be reevaluated. Here we discuss several evolutionary mechanisms and models which may affect our results.

Perhaps the most detailed examinations of these processes have been made by Hirayama, Tanaka, & Kogure (1978) and Hirayama (1978). In general their models predict that the intracluster gas can be in one of three states, depending upon the temperature of the gas ejected from the galaxies. If the temperature is less than 10^6 K, the gas flows toward the cluster center, while for temperatures greater than 3×10^8 K, the gas flows outward. At intermediate temperatures both inflow and outflow occur, with a stagnation radius between the two zones.

Hirayama (1978) has derived density, temperature, abundance, and iron K-line equivalent width distributions which constitute the most detailed predictions in the literature to date, and we have compared the Spartan 1 results with them. These predictions were produced under several assumptions. First, the mass-loss rate (per unit mass) per galaxy is assumed to be constant in both time and position with the value of $3 \times 10^{-19}\ \mathrm{s}^{-1}$ (Huchtmeier et al. 1975). This would be the case, as described in the previous section, if mass loss were due to galactic winds only, although combinations of various mass-loss mechanisms are possible also. Second, a King model is used for the galaxy distribution with a normalization which assumes that the dark matter is associated with the galaxies. Third, the ejected gas leaves the galaxy with no significant residual velocity and is immediately mixed with the primordial gas. Fourth, the primordial gas in the cluster-forming region is uniform initially and may have a density greater than the closure density of the universe, which is $5 \times 10^{-30}\ \mathrm{g\ cm}^{-3}$ for the value of the Hubble constant we have assumed (50 km s^{-1} Mpc^{-1}). This last assumption is not unrealistic given that clusters may condense out of large-scale overdense regions. Hirayama's predictions are functions of the temperature of the interstellar gas which is ejected from the galaxies and of the initial primordial gas density.

In Figure 6*a* we compare the Spartan 1 abundance envelope shown in Fig. 5*b* to the abundance distributions predicted by these models, in which the ejection temperature is 10^6 K and the initial primordial gas density is varied between 10^{-28} and $10^{-30}\ \mathrm{g\ cm}^{-3}$. Hirayama (1978) used a value of 3×10^{-5} for the solar number density of iron relative to hydrogen, and we have adjusted our results to this value. Also, in Figure 3 of Hirayama (1978) the predictions show the abundance of iron relative to that of the ejected gas. We have assumed a value of $1.0\ A_\odot$ for the abundance of the ejected gas and recalculated the ordinate in his plot in units of solar abundance. The Spartan 1 best-fit abundance is significantly steeper than most predicted profiles, although the 90% confidence envelope is consistent over the range 0–2 Mpc with the predicted profile which assumes a value of $10^{-28}\ \mathrm{g\ cm}^{-3}$ ($\sim 6 \times 10^{-5}\ \mathrm{cm}^{-3}$) for the primordial density. Lower values of primordial density at this ejection temperature are excluded by our results. Hirayama (1978) calculated models for only one other gas ejection temperature, 3×10^8 K (Fig. 4 of that work), for which the Spartan 1 abundance envelope implies a primordial density even higher than $10^{-28}\ \mathrm{g\ cm}^{-3}$.

In Figure 6*b* we show the predicted density and temperature distributions (Hirayama 1978) for the case in which the primordial gas density is $10^{-28}\ \mathrm{g\ cm}^{-3}$ and the ejection temperature is 10^6 K, and compare these predictions to the results obtained from the Spartan 1 best-fit model. The density in these predictions is normalized to produce the total X-ray luminosity of the Coma cluster. In Figure 6*b* we have reduced the Spartan 1 best-fit model density a factor of $(2)^{1/2}$ to approximate conditions in the Coma cluster ($L_x \propto \rho^2$). The Spartan 1

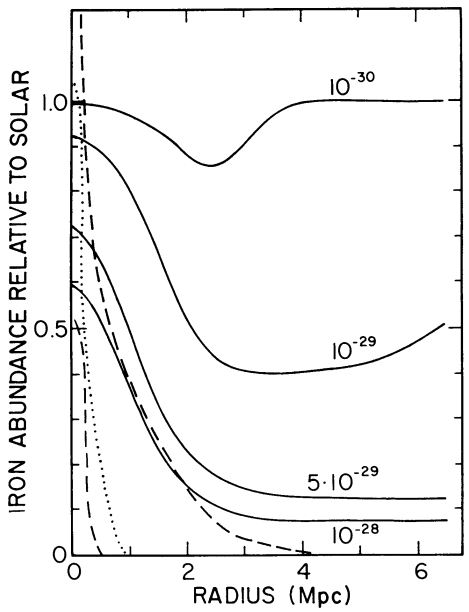

FIG. 6a

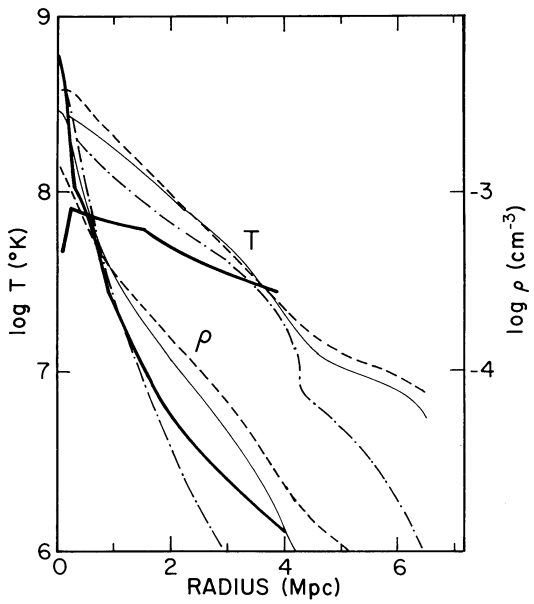

FIG. 6b

FIG. 6.—(*a*) Comparison between the Spartan 1 abundance results and the predicted distributions taken from Fig. 3 of Hirayama (1978), in which the temperature of the gas ejected from the galaxies was 10^6 K. Predicted distributions (*solid lines*) were calculated for values of the primordial gas density ranging between 10^{-28} and 10^{-30} g cm^{-3}. The Spartan 1 best-fit result (*dotted line*) and 90% confidence envelope (*dashed lines*) were taken from Fig. 5*b* and adjusted to a value of 3×10^{-5} for the solar number density of iron relative to hydrogen. To compare the predictions to our measurements, we have assumed the iron abundance of gas ejected from the galaxies is 1.0 A_0 (see text). (*b*) Comparison between the Spartan 1 best-fit density and temperature results (*solid lines*) and the predicted distributions taken from Fig. 1 of Hirayama (1978), in which the temperature of the gas ejected from the galaxies was 10^6 K and the primordial gas density was 10^{28} g cm^{-3} (*thin solid lines*). The Spartan 1 best-fit results were taken from Table 1, and the density was adjusted to account for the luminosity scaling used in the predictions (see text). Also plotted are the predicted distributions (Hirayama 1978) for a model where all the intracluster gas was ejected from galaxies (*dash-dot lines*) and for a model where all the intracluster gas is primordial (*dashed lines*).

density lies mostly within the envelope defined by the extreme cases where the intracluster gas is either of completely galactic or completely primordial origin. Differences between the Spartan 1 result and the prediction in which the primordial density is 10^{-28} g cm^{-3} are never more than a factor of 2. The Spartan 1 temperature profile is both cooler and flatter than the predicted temperature distribution. Most observed cluster temperatures are cooler than the predicted values (cf. Sarazin 1986), and there are only a limited number of measurements of temperature gradients in the intracluster gas (Snyder et al. 1990; Ponman et al. 1990; Edge 1989; Hughes 1991; Hughes, Gorenstein, & Fabricant 1988a). A satisfactory model to explain such flat temperature distributions, which might include such processes as cooling flows, cluster mergers, and thermal conduction, has yet to be developed.

In conclusion, the abundance gradient in the Perseus cluster, as measured by Spartan 1, is significantly steeper than Hirayama's evolutionary models, emphasizing the need for invoking mass-loss mechanisms, such as stripping, which work more effectively in the cluster core. However, the measured temperature gradient is significantly flatter. The density profile fits well those predictions of theory in which the initial density of primordial gas is 10^{-28} g cm^{-3} in the cluster formation region, a value well above the closure density.

Diffusive sedimentation of heavy elements toward the cluster core is another evolutionary mechanism which may produce an abundance gradient. Fabian & Pringle (1977) first considered this process and concluded that abundance gradients could arise even if the ejection rate of heavy elements from galaxies were constant thoughout the cluster. Different abundance gradients were predicted for different elements. However, Rephaeli (1978) has argued that Fabian & Pringle (1977) overestimate drift velocities, having neglected both collisions with helium and the strong inhibiting effects of cluster magnetic fields. Rephaeli (1978) concludes that diffusive sedimentation would require much more than a Hubble time, and thus the present observed abundance distribution in clusters should be constant with radius.

Abramopoulos, Chanan, & Ku (1981) have approached the question of evolution with a fresh perspective by investigating the distribution of elements obtained when a cluster has reached the limiting case of full equilibrium, regardless of whether there has been enough time to achieve this state. In their model each element has a different radial distribution, and high central abundances and steep gradients are predicted for all elements heavier than helium. At the cluster center the ratio of the iron density to the hydrogen density is about 0.16, roughly 4000 times the solar value, and drops to less than 0.006 $A_\odot$ at 0.75 core radii, in great disagreement with results from Spartan 1 as well as other instruments. However, in our analysis the abundance of all atoms heavier than helium was varied by the same factor as iron. Thus, from Figure 1*a* in their work, we have calculated the density relative to hydrogen (solar units) of the sum of all elements heavier than helium. The resulting central abundance and gradient are still too large, but the distribution does drop to small values at about 1.5 core radii, a value in good agreement with the Spartan 1 results (Table 1, Figs. 1 and 5). This suggests that although the Perseus cluster may not be in equilibrium at radii greater than 1 Mpc, it evolves toward this state is a manner that increases the

abundance of elements within about 1.5 core radii (0.6 Mpc). Nepveu (1981b) found that the value of the radius should not change with time.

We have also calculated the total predicted equilibrium density of all elements from Figure 1*a* of Abramopoulos et al. (1981) and find agreement between this result and the Spartan 1 best-fit model density outside of the cooling flow region ($r > 0.2$ Mpc). Uncertainties in the derived Spartan 1 density are too large to decide unambiguously between their theoretical density models which assume constant abundance and those which include gradients. However, taken together with the large departures from equilibrium in the observed abundance distribution, this result suggests that abundance measurements may be more sensitive to departures from equilibrium than density measurements. This sensitivity might be exploited in instruments of higher spectral resolution which can identify lines of many elements, where measurements of several elements might be used together to determine the degree of equilibrium attained within the cluster. One caveat is that the high central abundance of some elements such as oxygen could be produced by an early population of short-lived, massive stars (Type II supernovae), which may have oxygen-rich ejecta (Canizares et al. 1988; David et al. 1991).

4.2. *Comparison to Other Clusters*

Only two other clusters have been examined for the presence of abundance gradients, Virgo and Coma. Scanning observations of Virgo have been made with the *Ginga* satellite where the beam size was 1° FWHM in the scan direction (Koyama, Takano, & Tawara 1991). Fits of thermal models to the surface brightness data along the scan path yield an abundance of 0.5 $A_\odot$ at the cluster center and a drop to about 0.1 $A_\odot$ at radii greater than 2°. However, the angular distribution of abundance is comparable to the collimator profile; therefore no measurement of the abundance profile was possible. Observations of the Coma cluster has been made with *EXOSAT* (ME), *Tenma*, *Ginga*, and Spacelab 2 (Hughes 1991; Hughes et al. 1988a; Ponman et al. 1991). These instruments have collimators with wide fields of different sizes, and this provides a degree of spatial resolution. Additional observations with *EXOSAT* were made of fields offset from the cluster center. A comparison of the results of fitting thermal models to these data shows no evidence for an abundance gradient, and the average abundance is about 0.24 $A_\odot$.

It is premature to search for trends with only three objects, but is is interesting to note that both clusters with established abundance gradients, Virgo and Perseus, have cooling flows, while Coma has neither a cooling flow nor a gradient. Edge, Fabian, & Stewart (1991) have found that as many as 90% of all clusters may contain cooling flows, and those which do not may have had their cooling flows disrupted by merger events. Under this assumption, Ponman et al. (1991) have speculated that the lack of an abundance gradient in Coma may be the result of the same merger event which disrupted its cooling flow. Recent *ROSAT* observations of the Coma cluster have found evidence for the beginning of a merger (Briel, Henry, & Bohringer 1991). However, *ROSAT* observations also suggest that Perseus may be undergoing a merger (Schwarz et al. 1992), and this provides a counterexample to Ponman's hypothesis. It is not possible to determine with the present data whether the Coma and Perseus clusters are evolving in a significantly different manner, or whether the observed differences are transient. What is clear is the clusters are evolving dramatically at this epoch.

4.3. *The Mass Distribution of Iron*

Fabian & Pringle (1977) were among the first to suggest that clusters with abundance gradients would require a smaller total mass of iron to produce the observed iron line strength than clusters with constant abundance, and Abramopoulos et al. (1981) showed that this reduction in the total mass of heavy elements for the Coma cluster could be as high as a factor of 20. In Figure 7 we show the cumulative distributions of iron as a function of radius for the best-fit Spartan 1 model using a linear (Table 1) and a Gaussian abundance distribution. The distributions are very similar to each other, and the total masses of iron integrated out to a radius of 1.6 Mpc agree to within a factor of 2. These results are also in relatively good agreement with the iron mass distributions derived from the Spacelab 2 data (Ponman et al. 1990), even though the abundance distributions disagree.

The total mass of iron at radii less than 1.6 Mpc is about $3 \times 10^{10}\ M_\odot$, and this value is a factor of 5 smaller than the amount that would be present if the iron were uniformly distributed throughout the cluster with an average abundance of 0.5 $A_\odot$. To account for this iron mass roughly $1.3 \times 10^{13}\ M_\odot$ of gas at 1 $A_\odot$ must have been removed from galaxies. Lea & De Young (1976) and Himmes & Biermann (1980) found that ram pressure stripping could account for a few times $10^{13}\ M_\odot$ in a Hubble time. Similarly, a number of studies (Ikeuchi 1977; De Young 1978; Rephaeli 1978) have found that galactic winds are capable of providing as much as $10^{14}\ M_\odot$ of gas in a Hubble time, an amount which would be sufficient to account for the iron mass regardless of its distribution. Finally, we have calculated the total mass evaporated over a Hubble time for the heat conduction model using the mass-loss rates given by Cowie & Songaila (1977) convolved with a King distribution of galaxies, and we have obtained values of a few $\times 10^{14}\ M_\odot$ for core radii between 0.12 and 0.34 Mpc. In summary, all gas-removal mechanisms seem able to produce sufficient quantities of gas to account for the total mass of iron.

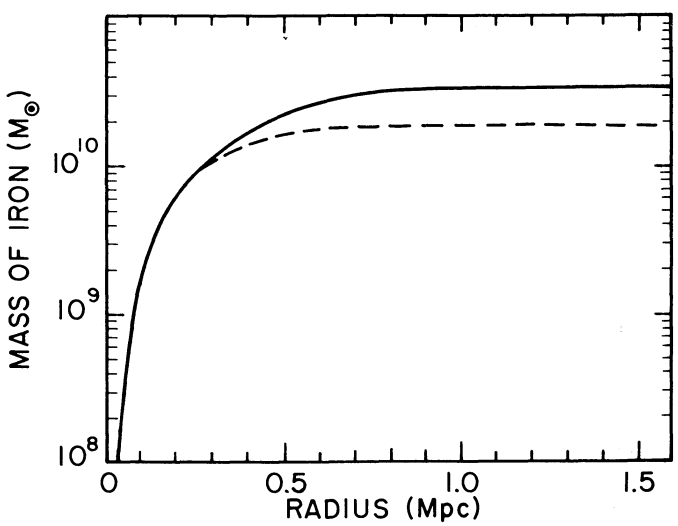

FIG. 7.—Cumulative distribution of iron as a function of radius for the best-fit Spartan 1 model (Table 1) using a linear (*solid line*) and a Gaussian abundance (*dashed line*) distribution.

5. CONCLUSIONS

The Spartan 1 instrument has resolved the spatial and spectral distribution of the 1–10 keV X-ray emission from the Perseus cluster in a region extending 50′ (1.6 Mpc) from the center. The data were fitted with a spherically symmetric three-dimensional model which included separate components for the cooling flow, extended cluster emission, and a possible point source located at NGC 1275. The best-fit model assumed a power-law temperature distribution and a modified King density distribution for the cooling flow component. The extended cluster emission was modeled with a separate modified King density and a polytropic temperature-density relation. The point source was modeled with a power law. We summarize the major conclusions of our study:

1. A careful analysis has been made of the abundance distribution of iron as a function of radius. We confirm the existence of a gradient, in which the best-fit abundance is $0.77^{+0.30}_{-0.38}$ $A_\odot$ at the center and the linear gradient is $-1.10^{+0.89}_{-2.24}$ $A_\odot$ Mpc^{-1} (90% confidence for a single interesting parameter). This result is in agreement with the values we reported in Ulmer et al. (1987), which were derived from fits to slices from the surface brightness distribution. Although the Spacelab 2 results also show evidence of an abundance gradient, their central abundance is higher and their gradient is steeper. This discrepancy may be due to a variable point source of iron K-line emission in NGC 1275. Observations made by the BBXRT high-resolution spectrometer cannot rule out the gradient reported here. However, our results disagree with the constant abundance derived from *Ginga* observations.

2. Joint 90% confidence limits to the abundance parameters have been produced, and the resulting limits to the abundance distribution have been applied to theoretical models of cluster structure and evolution. The Spartan 1 results are consistent with a gas removal mechanism with enhanced efficiency at the cluster center, and either ram-pressure stripping and/or thermal evaporation models are consistent with the data. However, we cannot rule out the presence of a portion of the ejected gas being produced by galactic winds. A measure of agreement is found between the Spartan 1 results and the cluster evolution models of Hirayama (1978), for cases in which the initial density of primordial gas in the cluster formation region is high ($\geq 10^{-28}$ g cm^{-3}).

3. The integrated mass of iron out to a radius of 1.6 Mpc (50′) is about 3×10^{10} $M_\odot$. This value is about 5 times smaller than that deduced from X-ray observations under the assumption of a constant abundance.

4. In the outer regions of the cluster, the core radius and exponent of the best-fit modified King model density are $0.41^{+0.29}_{-0.07}$ Mpc and $1.09^{+0.36}_{-0.09}$, respectively, in agreement with those given in Snyder et al. (1990). The best-fit polytropic exponent, $1.12^{+0.36}_{-0.04}$, indicates that the gas is close to being isothermal outside the cooling flow out to distances of at least 1.6 Mpc. In addition, Spartan 1 results have revealed significant asymmetries in the temperature and density distributions at large radii (Snyder et al. 1990).

We thank Brad Stuart, Alexander Cocran, and Robert DeMajistre for assistance in modification of the cluster modeling code, John Raymond for a copy of his plasma emissivity code, and Len Cowie and Gary Chanan for discussion of their articles. We are indebted greatly to Trevor Ponman for many stimulating discussions, for suggesting tests of the Spartan 1 results, and for performing extensive tests at our request on the Spacelab 2 results. We thank Richard Mushotzky, Jack Hughes, Craig Sarazin, and Steven Allen for scientific discussion and comments on the manuscript.

REFERENCES

Abramopoulos, F., Chanan, G. A., & Ku, W. H.-M. 1981, ApJ, 248, 429
Allen, S. W., Fabian, A. C., Johnstone, R. M., Nulsen, P. E. J., & Edge, A. C. 1992, MNRAS, 254, 51
Branduardi-Raymont, G., Fabricant, D., Feigelson, E., Gorenstein, P., Grindlay, J., Soltan, A., & Zamorani, G. 1981, ApJ, 248, 55
Branduardi-Raymont, G., Kellett, B., Fabian, A. C., McGlynn, T., Manzo, G., & Peacock, A. 1985, Adv. Space Res., 5, 133
Briel, U. G., Henry, J. P., & Bohringer, H. 1991, in Clusters and Superclusters of Galaxies (Contributed Talks and Poster Papers), ed. M. M. Colless, A. Babul, A. C. Edge, R. M. Johnstone, & S. Raychaudhury (Cambridge: Institute of Astronomy), 91
Brown, R. L., & Gould, R. J. 1970, Phys. Rev. D, 8, 2252
Canizares, C. R., Markert, T. H., & Dohahue, E. 1988, in Cooling Flows and Clusters of Galaxies, ed. A. C. Fabian (Dordrecht: Kluwer), 63
Cowie, L. L., & Songaila, A. 1977, Nature, 266, 501
Cruddace, R. G., et al. 1989, NRL Rep. 9207
David, L. P., Arnaud, K. A., Forman, W., & Jones, C. 1990, ApJ, 356, 32
David, L. P., Forman, W. A., & Jones, C. 1991, ApJ, 380, 39
David, L. P., Hughes, J. P., & Tucker, W. H. 1992, ApJ, 394, 452
De Young, D. S. 1978, ApJ, 223, 47
Edge, A. C. 1989, Ph.D. thesis, Leicester Univ.
Edge, A. C., Fabian, A. C., & Stewart, G. C. 1991, in Clusters and Superclusters of Galaxies (Contributed Talks and Poster Papers), ed. M. M. Colless, A. Babul, A. C. Edge, R. M. Johnstone, & S. Raychaudhury (Cambridge: Institute of Astronomy), 35
Eyles, C. J., Watt, M. P., Bertram, D., Church, M. J., Ponman, T. J., Skinner, G. K., & Willmore, A. P. 1991, ApJ, 376, 23
Fabian, A. C., Hu, E. M., Cowie, L. L., & Grindlay, J. 1981, ApJ, 248, 47
Fabian, A. C., & Pringle, J. E. 1977, MNRAS, 181, 5P
Fritz, G. G., Cruddace, R. G., Snyder, W. A., & Kowalski, M. P. 1993, in preparation
Gaetz, T. J., Salpeter, E. E., & Shaviv, G. 1987, ApJ, 316, 530
Gisler, G. R. 1976, A&A, 51, 137
———. 1979, ApJ, 228, 385
Gorenstein, P., Fabricant, D., Topka, K., Harnden, F. R., Jr., & Tucker, W. H. 1978, ApJ, 224, 718
Gunn, J. E., & Gott, J. R., III. 1972, ApJ, 176, 1
Heiles, C. 1975, A&AS, 20, 37
Henriksen, M. J. 1985, Ph.D. thesis, Univ. Maryland
Himmes, A., & Biermann, P. 1980, A&A, 86, 11
Hirayama, Y., Tanaka, Y., & Kogure, T. 1978, Prog. Theor. Phys., 59, 751
Hirayama, Y., & Ikeuchi, S. 1978, Prog. Theor. Phys., 60, 1337
Hirayama, Y. 1978, Prog. Theor. Phys., 60, 724
Huchtmeier, W. K., Tammann, G. A., & Wendker, H. J. 1975, A&A, 42, 205
Hughes, J. P. 1991, in Iron Line Diagnostics in X-Ray Sources, ed. A. Treves, G. C. Perola, & L. Stella (Berlin: Springer), 80
Hughes, J. P., Gorenstein, P., & Fabricant, D. 1988a, ApJ, 329, 82
Hughes, J. P., Yamashita, K., Okumura, Y., Tsunemi, H., & Matsuoka, M. 1988b, ApJ, 327, 615
Ikeuchi, S. 1977, Prog. Theor. Phys., 58, 1742
Jones, C., & Forman, W. 1984, ApJ, 276, 38
Kawai, N., Fenimore, E. E., Middleditch, J., Cruddace, R. G., Fritz, G. G., Snyder, W. A., & Ulmer, M. P. 1988, ApJ, 330, 130
Kent, S. M., & Sargent, W. L. W. 1983, AJ, 88, 697
Koyama, K., Takano, S., & Tawara, Y. 1991, Nature, 350, 135
Lampton, M., Margon, B., & Bowyer, S. 1976, ApJ, 208, 177
Lea, S. M., & De Young, D. S. 1976, ApJ, 210, 647
Malina, R., Lampton, M., & Bowyer, S. 1976, ApJ, 209, 678
Mathews, W. G., & Baker, J. C. 1971, ApJ, 170, 241
Mitchell, R. J., Culhane, J. L., Davison, P. J. N., & Ives, J. C. 1976, MNRAS, 176, 29P
Morini, M., et al. 1986, ApJ, 307, 486
Mushotzky, R. F. 1992, in Clusters and Superclusters of Galaxies (Invited Talks) (Cambridge: Institute of Astronomy), 91
Mushotzky, R. F., Holt, S. S., Smith, B. W., Boldt, E., & Serlemitsos, P. J. 1981, ApJ, 244, L47
Mushotzky, R. F., Marshall, F. E., Boldt, E. A., Holt, S. S., & Serlemitsos, P. J. 1980, ApJ, 235, 377
Nepveu, M. 1981a, A&A, 98, 65
———. 1981b, A&A, 101, 362
Petre, R. 1991, BAAS, 23, 841
Piro, L., Massaro, E., Perola, G. C., & Molteni, D. 1988, ApJ, 325, L25
Ponman, T. J. 1990, private communication

Ponman, T. J., Bertram, D., Church, M. J., Eyles, C. J., Watt, M. P., Skinner, G. K., & Willmore, A. P. 1990, Nature, 347, 450
Ponman, T. J., Watt, M. P., Knight, P. A., Bertram, D., Church, M. J., Eyles, C. J., Skinner, G. K., & Willmore, A. P. 1991, in Iron Line Diagnostics in X-Ray Sources, ed. A. Treves, G. C. Perola, & L. Stella (Berlin: Springer), 76
Primini, F. A., et al. 1981, ApJ, 243, L13
Raymond, J. C., & Smith, B. W. 1985, private communication
Rephaeli, Y. 1978, ApJ, 225, 335
Rothschild, R. E., Baity, W. A., Marscher, A. P., & Wheaton, W. A. 1981, ApJ, 243, L9
Sarazin, C. L. 1986, Rev. Mod. Phys., 58, 1
Schwarz, R. A., Edge, A. C., Voges, W., Bohringer, H., Ebeling, H., & Briel, U. 1992, A&A, 256, L11
Serlemitsos, P. J., Smith, B. W., Boldt, E. A., Holt, S. S., & Swank, J. H. 1977, ApJ, 211, L63
Snyder, W. A., Cruddace, R. G., Kowalski, M. P., Fritz, G. G., & Fenimore, E. E. 1991, in Iron Line Diagnostics in X-Ray Sources, ed. A. Treves, G. C. Perola, & L. Stella (Berlin: Springer), 53
Snyder, W. A., Kowalski, M. P., Cruddace, R. G., Fritz, G. G., Middleditch, J., Fenimore, E. E., Ulmer, M. P., & Majewski, S. R. 1990, ApJ, 365, 460
Takahara, F., & Ikeuchi, S. 1977, Prog. Theor. Phys., 58, 1728
Takeda, H., Nulsen, P. E. J., & Fabian, A. C. 1984, MNRAS, 208, 261
Ulmer, M. P., Cruddace, R. G., Fenimore, E. E., Fritz, G. G., & Snyder, W. A. 1987, ApJ, 319, 118
Veigele, W. M. J. 1973, Atomic Data Tables, 5, 51
White, D. A., Fabian, A. C., Johnstone, R. M., Mushotzky, R. F., & Arnaud, K. A. 1991, MNRAS, 252, 72
White, R. E., III 1991, ApJ, 367, 69